Journal of Experimental Pharmacology

Dovepress
Taylor & Francis Group

Open Access Full Text Article

ORIGINAL RESEARCH

Phytochemical Analysis, Computational Study, and in vitro Assay of *Etlingera elatior* Inflorescence Extract Towards Inducible Nitric Oxide Synthase

Deshanda Kurniawan Prayoga[1,*], Dian Ayu Eka Pitaloka[2,*], Diah Lia Aulifa[3,*], Arif Budiman[4,*], Jutti Levita[2*], Supat Jiranusornkul[5,*], Binh Phu Nguyen[6,*]

[1]Doctoral Program in Pharmacy, Faculty of Pharmacy, Universitas Padjadjaran, Sumedang, Indonesia; [2]Department of Pharmacology and Clinical Pharmacy, Faculty of Pharmacy, Universitas Padjadjaran, Sumedang, Indonesia; [3]Department of Pharmaceutical Analysis and Medicinal Chemistry, Faculty of Pharmacy, Universitas Padjadjaran, Sumedang, Indonesia; [4]Department of Pharmaceutics and Pharmaceutical Technology, Faculty of Pharmacy, Universitas Padjadjaran, Sumedang, Indonesia; [5]Department of Pharmaceutical Science, Faculty of Pharmacy, Chiang Mai University, Chiang Mai, Thailand; [6]School of Mathematics and Statistics, Victoria University of Wellington, Wellington, New Zealand

*These authors contributed equally to this work

Correspondence: Jutti Levita, Department of Pharmacology and Clinical Pharmacy, Faculty of Pharmacy, Universitas Padjadjaran, Sumedang, 46363, West Java, Indonesia, Email jutti.levita@unpad.ac.id

Background: Overproduction of nitric oxide (NO), catalyzed by inducible nitric oxide synthase (iNOS), in the gastric mucosa, contributes to the inflammatory process caused by oxidative stress. Current medications for gastric ulcers, such as proton pump inhibitors and histamine-2 receptor antagonists, have been reported to generate adverse reactions.

Purpose: To obtain the phytochemical profile of *Etlingera elatior* inflorescence extract, computational studies, and in vitro assay of the extract towards iNOS.

Methods: Fresh *E. elatior* inflorescence petals collected from West Java, Indonesia, were extracted using ethanol, and their nutritional composition, anthocyanin content, and levels of vitamin C, C3G, and quercetin in the extract were determined. Drug-likeness and ADMET properties were predicted, and the binding affinity and stability of the phytoconstituents towards iNOS were studied using molecular docking and molecular dynamic simulation, and in vitro assay of the extract towards human iNOS.

Results: The extract contains protein 21.81%, fat 0.99%, carbohydrate 38.27%, water 24.56%, and ash 14.37%. The total anthocyanin and vitamin C levels were 47.535 mg/100 g and 985.250 mg/100 g, respectively. The levels of C3G and quercetin were 0.0007% w/w, 0.004% w/w, and 0.0005% w/w, respectively. Drug-likeness and ADMET properties of the constituents showed that most followed Lipinski Rules of Five (Ro5), with few violations. All phytoconstituents occupied the catalytic site by binding to Glu377, and Trp372, similar to *S*-ethylisothiourea (SEITU) and quinazoline, the iNOS inhibitors. Among these, the flavylium cation of cyanidin, demethoxycurcumin, C3G, cyanidin, and quercetin showed the best binding affinities. Root mean square deviation (RMSD), root mean square fluctuation (RMSF), solvent-accessible surface area (SASA), and radius of gyration (Rg) graphs confirmed the stability of the complexes. *E. elatior* inflorescence extract inhibited human iNOS with an IC50 value of 24.718 µg/mL.

Conclusion: *Etlingera elatior* inflorescence may inhibit iNOS activity due to its anthocyanin and flavonoid content. The flavylium cation of cyanidin, demethoxycurcumin, C3G, cyanidin, and quercetin play leading roles in the interaction with iNOS.

Keywords: anti-inflammation, cyanidin-3-glucoside, polyphenols, proximate analysis, quercetin

Introduction

Gastric ulcers are common and frequent distressing ailments characterized by open sores or lesions in the (1) lining of the lower part of the esophagus (cardiac zone), (2) corpus zone, or (3) upper part of the small intestine. Ulcers form when cells on the surface of the lining become inflamed and die.[1–3] Gastric ulcers are global problems with a lifetime risk of development. The incidence of gastric ulcer is 2.4% (487 cases of 20,006 upper gastrointestinal endoscopies) in the Dutch population,[4] and the global annual incidence in 2009, reported in a systematic review article, was 0.10% to 0.19% based on physician-

Received: 9 November 2024
Accepted: 11 December 2024
Published: 8 March 2025

diagnosed and 0.03% to 0.17% based on hospitalization data.[5] An epidemiological study in Shanghai, China, of 3153 participants, the prevalence of *Helicobacter pylori* infection was 73.3% and gastric ulcer is as high as 17.2%.[6] These ulcers may lead to an imbalance in homeostasis due to excessive reactive radical compounds, such as nitric oxide (˙NO), nitrogen dioxide ($^{\cdot}NO_2$), and nonradical compounds, eg, peroxynitrite ($ONOO^-$) and dinitrogen trioxide (N_2O_3).[7]

Nitric oxide (·NO) production is catalyzed by nitric oxide synthase (NOS), a heme-containing monooxygenase. There are three different isozymes of NOS, the constitutively expressed neuronal NOS (nNOS), the endothelial NOS (eNOS), and the endotoxin or cytotoxin-inducible NOS (iNOS).[8] NOS catalyzes the oxidation of its substrate, L-arginine, to an intermediate, N-hydroxy-L-arginine, followed by the production of L-citrulline and radical NO.[9] Excessive NO produced by iNOS contributes to both gastric mucosal defense and damage and has been implicated in tissue injury in patients with peptic ulcers. In contrast, physiological NO produced by nNOS and eNOS preserves gastric mucosal integrity by controlling mucosal blood flow, epithelial secretion, and barrier function.[10]

The human iNOS oxygenase domain (residues 82–508) is elongated by an α–β fold and the heme group is preserved at the center of the protein interior, which provides considerable Van der Waals interactions with hydrophobic and aliphatic side chains. Heme iron is penta-coordinated and axially coordinated to proximal Cys200. Two aromatic residues, Trp194 and Phe369, fit the porphyrin ring. The substrate, L-arginine, attaches to the narrow part of the catalytic site cavity with the guanidino group lying coplanar to the heme and builds two hydrogen bonds to both carboxy oxygens of Glu377, positioning the substrate above the heme, thus making this residue critical for substrate binding.[11] The structure of the oxygenase domain of human iNOS with an inhibitor, S-ethylisothiourea (SEITU), has described a structural basis for interpreting the binding mode of this inhibitor with iNOS. The ethyl group of SEITU is positioned near the heme and Phe369 side chains, confirming that the ethyl group of inhibitors is essential for the inhibition of NOS activity.[11,12]

Numerous studies have reported that plant flavonoids can inhibit NOS and eventually decrease excessive NO production.[13–17] An in vitro study described the structural requirements of flavonoids for inhibiting NO production preferably possessing flavones, without glycoside moiety, having a hydroxyl group at the B ring and a catechol group.[13] The flavonoids and isoflavonoid glycosides from the rhizomes of *Iris spuria* L. could inhibit iNOS.[14] Human aortic cells pretreated with flavonoids, eg, quercetin, resveratrol, and proanthocyanidin, indicated a decrease in reactive oxygen species (ROS) induced by high glucotoxicity conditions.[15] Flavonoids rutin and quercetin could inhibit lipopolysaccharide-exposed NO production in mouse macrophage cell lines (RAW 264.7) in a concentration-dependent manner without cytotoxicity.[16] The important amino acid residues in the iNOS catalytic pocket that contribute to its catalytic reactions were Glu296, Trp346, Tyr347, Val352, Phe369, Tyr373, Glu377, and Asp382, as reported by previous molecular docking studies, thus molecular interaction with these residues may result in the enzyme inhibition.[17–19]

Etlingera elatior of the family Zingiberaceae has been reported to contain abundant polyphenols, flavonoids, anthocyanins, and steroids, in various parts of the plant. The inflorescences of *E. elatior*, which have a sour taste, were reported to contain 286 mg/kg of kaempferol and 21 mg/kg of quercetin.[20–22] The acetone extract of *E. elatior* inflorescence contained total phenols of 687.0 mg gallic acid equivalence (GAE) per 100 g extract and total flavonoids of 1431 mg quercetin equivalence (QE) per 100 g extract, while the methanol extract showed total anthocyanins of 5.9 mg cyanidin-3-glucoside equivalence (C3GE) per 100 g extract.[23] The ethanol extract of *E. elatior* inflorescence petals exhibited anti-inflammatory activity by downregulating the expression of NF-kappaB-p65 in gastric ulcer-induced rats.[24] However, none of these studies reported the effects of *E. elatior* inflorescence petals on iNOS or their phytochemical profiles. Considering all, our study aimed to determine the nutritional composition, anthocyanin content, vitamin C, C3G, and quercetin in *E. elatior* inflorescence petals collected in West Java, Indonesia, and to identify the binding mode, affinity, and stability of their known phytoconstituents toward human iNOS. *E. elatior* inflorescence petals were chosen for the sample materials because they have a strong red color, probably due to their abundant polyphenols, flavonoids, and anthocyanins.

Materials and Methods

Plant Materials and Preparation of E. elatior Inflorescence Extract (EEIE)

Fresh *Etlingera elatior* inflorescence petals were collected from West Java, Indonesia, and authenticated by Arifin Surya Dwipa Irsyam (https://www.scopus.com/authid/detail.uri?authorId=57211286941; https://herbarium.sith.itb.ac.id/profil-kurator/),

a certified botanist at the School of Life Sciences and Technology, Bandung Institute of Technology (Bandung, West Java, Indonesia) (https://herbarium.sith.itb.ac.id/koleksi/). The material was confirmed to be *Etlingera elatior* (Jack) R.M.Sm. of the Zingiberaceae family (document number 74/IT1.C11.2/TA.00/2024) with characteristics that matched those described in the references.[25,26]

EEIE was prepared according to previously described methods with some modifications.[24,27] Briefly, fresh inflorescence petals of *E. elatior* were thoroughly examined to exclude damaged or crushed parts. The petals were washed under running water to remove dirt and other contaminants, dried in an oven at 45–50 °C for 24 h, ground into a coarse powder, and sieved using a Mesh-12 sieve. Approximately 1300 g of the coarse powder was cold extracted using 70% ethanol at a ratio of 1:10 (w/v) for 3×24 h. Ethanol 70% was chosen by considering its universal properties to dissolve various phytoconstituents. The liquid extracts were collected, filtered, and evaporated in a vacuum rotary evaporator (Büchi) at 50 °C until a viscous extract of EEIE was yielded (20.2% w/w).

Analysis of the Nutritional Composition, Vitamin C, and Total Anthocyanins of EEIE

The nutritional composition of EEIE was analyzed by following Official Methods of Analysis 2023 (https://www.aoac.org/official-methods-of-analysis/):[28]

Water content was determined based on the weight lost during heating at 102 ± 2 °C in an oven for 2 h. Approximately 1 g of EEIE was weighed and placed in a constant-weight dry crucible, followed by drying at 105 °C for 3 h. After drying, the crucible was cooled in a desiccator and weighed. This process was repeated until a constant weight was achieved. The water content in EEIE was calculated using the following equation:

$$Water\ Content\ (\%) = \frac{W_1 - W_2}{W_1 - W_0} \times 100\%$$

where W_0 is = the weight of the bottle and cap (g); W_1 is = the weight of the bottle + cap + EEIE before drying (g); W_2 is = the weight of the bottle + cap + EEIE after drying (g).

Ash content was determined based on the principle that organic substances decompose into water and carbon dioxide (CO_2). Approximately 2 g of EEIE was weighed, placed in a constant-weight dry crucible, and charred over a burner flame. The crucible was transferred to a furnace set at 550 °C, heated for 3–4 h to complete combustion, cooled in a desiccator, and weighed. The ash content in EEIE was calculated using the following equation:

$$Ash\ Content\ (\%) = \frac{W_1 - W_2}{W} \times 100\%$$

where W = EEIE weight before combustion (g); W_1 = EEIE + crucible weight after combustion (g); W_2 = crucible weight (g).

Protein content was determined using the semi-micro Kjeldahl method as follows: 0.1 g EEIE was weighed and placed in a Kjeldahl flask, and 0.5 g of a selenium mixture (SeOz: K_2O_4: $CuSO_4.5H_2O$ in a 1:40:8 ratio) was added. The mixture was digested over a burner flame for approximately 2 h until the solution boiled and became green. The contents of the flask were then transferred to a 100 mL volumetric flask, and distilled water was added. A 5 mL aliquot of this solution was pipetted into the distillation apparatus, followed by 5 mL of 30% NaOH, and a few drops of phenolphthalein indicator. The distillation process was carried out for 10 min, with 10 mL of a 2% boric acid solution mixed with bromocresol green-methyl red used as the receiving solution. The distillate was titrated with standardized 0.01 N HCl until a color change was observed. The protein content in EEIE is calculated using the following equation:

$$Protein\ Content\ (\%) = \frac{(V_1 - V_2) \times N \times 0.014 \times Cf \times Df}{W} \times 100\%$$

where W = weight of EEIE (g); V_1 is = the volume of HCl 0.01 N used in EEIE titration (mL); V_2 is = the volume of HCl 0.01 N used in blank titration (mL); N = HCl normality; Cf = conversion factor to protein from a sample (generally using 6.25); and Df = dilution factor.

Fat content was determined using the Soxhlet method. The principle of this method involves extracting the fat from the sample using a solvent and then determining the weight of the fat recovered. Approximately 1 g of EEIE was

wrapped in filter paper and placed in a Soxhlet flask that had been pre-weighed, hexane was added, and the mixture was extracted for 6 h. After extraction, the Soxhlet flask was placed in an oven at 105 °C to evaporate the solvent, cooled in a desiccator, and weighed to determine fat content. The fat content in EEIE was calculated using the following equation:

$$Crude\ Fat\ Content\ (\%) = \frac{(W_2 - W_1) \times 100}{S}$$

where S = weight of EEIE (g); W = weight of the empty flask (g); W_2 = weight of the flask + EEIE (g)

Carbohydrate content was determined by subtracting the total percentages of protein and fat 100%. The carbohydrate content in EEIE was calculated using the following equation:

$$Carbohydrate\ Content\ (\%) = 100\% - (\%\,MC + \%\,AC + \%\,CP + \%\,Fat\ content)$$

where, MC = moisture content; AC = ash content; and CP = crude protein

The level of vitamin C was determined using the iodometric titration method,[29] and the total anthocyanins were quantified using the pH differential spectrophotometric method,[30] as follows: EEIE was mixed well with 20 mL of 0.025 M potassium chloride buffer (pH 1.0) and another EEIE with 0.4 M sodium acetate buffer (pH 4.5). The mixtures were left to react for 20 min at room temperature and centrifuged at 7000 rpm for 15 min at 4 °C. The absorbance of the supernatants was measured at 520 nm and 700 nm. The total anthocyanins in EEIE (TAC) were calculated using the following formula:

$$TAC\ (\%) = \frac{A\,x\,MW\,x\,DF\,x\,V}{\epsilon\,x\,l\,x\,M} \times 100$$

where A = (A_{520} nm − A_{700} nm) pH 1.0 − (A_{520} nm − A_{700} nm) pH 4.5; ϵ is the molar absorptivity of cyanidin-3-glucoside; l = path length in cm; DF = dilution factor; MW = the molecular weight of cyanidin-3-glucoside (449.2 g/mol); V = volume of extract (mL); and M = fresh mass of the sample (g).

Analysis of C3G and Quercetin in EEIE

EEIE was analyzed by thin-layer chromatography (TLC)-densitometry following a method previously described by Doshi and Une et al in 2016.[31] Approximately 10 g of EEIE was placed in an evaporating dish and dissolved in 100 mL of analytical-grade methanol solvent. For the standards, approximately 1 mg of C3G standard, and 10 mg of quercetin standard were each dissolved in 10 mL of analytical-grade ethanol solvent. Both standard solutions and samples were filtered using Whatman filter paper no. 41 before spotting onto a TLC plate (Silica gel 60 F254, 10 cm). The TLC plate was then spotted with varying concentrations of the standards, specifically C3G (5, 10, 15, 20, and 25 µg/mL), and quercetin (25, 50, 75, 100, and 125 µg/mL). The plate was inserted into a chamber saturated with a mixture of n-butanol: formic acid: water (65:19:16), and toluene: ethyl acetate: formic acid (5:4:0.5) for quercetin as the mobile phase, eluted to the finish line, dried, and examined under UV lights and analyzed using TLC-Densitometry at the maximum wavelengths of 520–570 nm for C3G and 280–320 nm for quercetin.[32] The data for each peak, including area and Rf values, were recorded, and the concentrations of C3G and quercetin were quantified using a linearity curve and regression equation.

In silico Pharmacology (Computational Simulation)

Hardware and Software

The hardware is a personal computer with specifications AMD Ryzen™ 5 5600H CPU @ 3.3GHz (8 CPUs), Windows 11 Home 64-bit Operating system, 512 GB hard disk capacity, and 8169 MB RAM. The software is ChemDraw Ultra 12.0 program free trial version; AutoDock 4.5.6 in the MGLTools 1.5.6 program package of the Molecular Graphics Laboratory (MGL) by the Scripps Research Institute (http://mgltools.scripps.edu/) to prepare the molecular docking and stimulate the process of docking of the ligands with the enzyme; Open Babel 2.4.1 (http://openbabel.org) to change the file format during the research process; Discovery Studio Visualizer 4.5 (copyright 2021, Accelrys Software Inc.) to visualize and analyze the results of ligands and proteins; and PyMOL v.1.6.X program to visualize the superimposition of the native ligands.

Preparation of the Macromolecule and the Ligands

Macromolecule preparation was carried out according to Aulifa et al in 2022 with modifications.[33] The 3D crystal structure of human iNOS with inhibitor (PDB ID 4NOS; PDB: 10.2210/pdb4NOS/pdb; resolution of 2.25 Å; R-free value of 0.289; R-work value of 0.199; deposited by Fischmann et al, 1999) was downloaded from the Protein Data Bank (https://www.rcsb.org/structure/4NOS). Crystallographic R-free and R-work values indicate the ability of macromolecular structure models to explain the quality of the crystallographic data on which they are based. A lower R-free value is likely to be regarded more favorably.[34] The macromolecule was analyzed for its active site and ligand interaction and prepared for the molecular docking simulation by adding polar hydrogen atoms and Kollman charges using AutoDockTools.

The ligands are quercetin (molecular formula: $C_{15}H_{10}O_7$; molecular weight: 302.23 g/mol), kaempferol (molecular formula: $C_{15}H_{10}O_6$; molecular weight: 286.24 g/mol), apigenin (molecular formula: $C_{15}H_{10}O_5$; molecular weight: 270.24 g/mol), luteolin (molecular formula: $C_{15}H_{10}O_6$; molecular weight: 286.24 g/mol), myricetin (molecular formula: $C_{15}H_{10}O_8$; molecular weight: 318.23 g/mol), rutin (molecular formula: $C_{27}H_{30}O_{16}$; molecular weight: 610.5 g/mol), cyanidin (molecular formula: $C_{15}H_{11}O_6$; molecular weight: 287.24 g/mol), and C3G (molecular formula: $C_{21}H_{21}ClO_{11}$; molecular weight: 484.8 g/mol), as described in earlier studies.[35–37] Quinazoline (PubChem CID 9210) and SEITU (PubChem CID 5139) were chosen as the standard drugs due to their activity in inhibiting NO production.[38–40] All these compounds were sourced from the PubChem database (https://pubchem.ncbi.nlm.nih.gov) and the Chem3D Ultra 12.0 was employed to build the ligands. The molecular mechanics MM2 method was employed to minimize the potential energy, and the PM3 (semi-empiric parametric 3 methods) to achieve the transition state. The ligands were further prepared for molecular docking simulations using the AutoDock 4.5.6 program by adding hydrogen atoms, merging the non-polar hydrogens, and assigning Gasteiger charges.

Prediction of the Drug-Likeness Profile by Applying the Lipinski Rules of Five

The drug-likeness profile and absorption of quercetin, kaempferol, apigenin, luteolin, myricetin, rutin, cyanidin, and C3G from *E. elatior* inflorescences by human body were predicted using the Lipinski rule of five (Ro5) (http://www.scfbio-iitd.res.in/software/drugdesign/lipinski.jsp). The requirements for drug-like molecules to be orally effective should meet at least four criteria of the Lipinski Ro5, including a molecular mass of less than 500, cLogP, hydrogen bond acceptors (HBAs), hydrogen bond donors (HBDs), and molar refractivity. In addition, the candidate compound must have a bioavailability value of at least 0.10–0.17, for optimum bioavailability.[41,42]

Molecular Docking Simulation

To validate the molecular docking program, the inhibitor S-ethyl thiourea (SEITU) co-crystallized in human iNOS, was extracted and subsequently re-docked into its original position. The re-docked conformation of the SEITU molecule was aligned with its respective origin (Figure 1), and the root mean square deviation (RMSD) was computed.[18,32,43] Molecular docking simulations were carried out using the AutoDock 4.5.6 program.

Calculation of ADMET Properties

Five of the ten phytoconstituents with the best affinity to human iNOS were further evaluated for their ADMET properties (absorption, distribution, metabolism, excretion, and toxicology). This analysis is carried out using the pkCSM program (https://biosig.lab.uq.edu.au/pkcsm/prediction_single). The flavonoid structure data were submitted to the program site. The parameters are the water solubility, % HIA (human intestinal absorption), Caco2 (Cancer coli-2), VDss (distribution volume at steady state), PPB (plasma protein binding), CYP3A4 inhibitor, CYP2D6 inhibitor, total clearance, renal organic cation transporter 2, the Ames toxicity, and LD_{50}.[44] The pkCSM program was chosen because it has shown higher accuracy (83.8%) compared to ToxTree (75.8%).[45]

Molecular Dynamic Simulation

MD simulations were performed using GROMACS (Groningen Machine for Chemical Simulation) 2016.3 software with the AMBER99SB-ILDN force field.[46] The topology and ligand parameters were generated using ACPYPE.[47] The particle mesh Ewald method was used to calculate the electrostatic force between particles at a given distance.[48] The system was neutralized

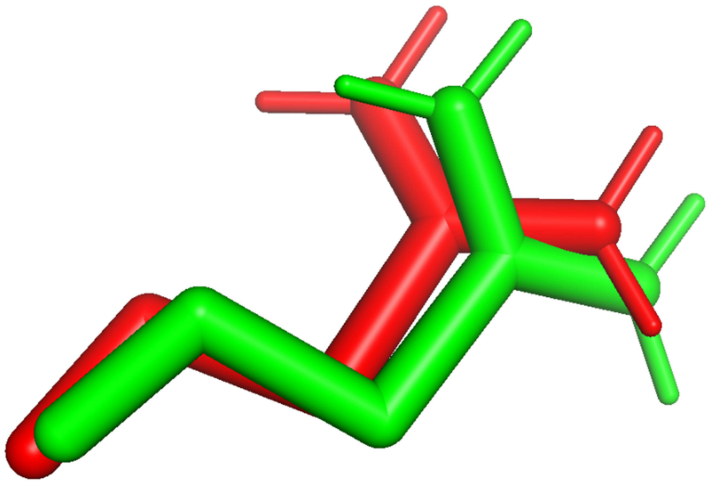

Figure 1 The superimposition of two molecules of SEITU (the green color molecule represents the docked- SEITU; the red color molecule represents the co-crystallized SEITU) in the catalytic pocket of iNOS. The obtained consecutive RMSD value is 1.303 Å.

using the NaCl model, by introducing Na+ and Cl^- ions, and the solvation process was carried out with the TIP3P water cube model.[49] The simulation preparation stage comprises the stages of minimizing, heating to 310°C, achieving temperature equilibrium, achieving pressure equilibrium, and thereafter proceeding with the simulation process. Subsequently, an MD production phase of 100 ns was carried out, utilizing a timestep of 2 fts. The functions grms, g_rmsf, and grg were used to calculate RMSD, RMSF, and radius of gyration (Rg). Following the MD simulation, the solvent-accessible surface area (SASA) is employed to determine the primary direction and magnitude of the dominating motion.[50–53]

The Inhibitory Activity of EEIE to Human iNOS by in vitro Study

The assay was performed following the procedure outlined in the iNOS Inhibitory Screening Kit (Catalogue No. EINO-100; EnzyChrom-BioAssay). Preparation was done with various concentrations of EEIE (100, 200, 400, and 500 µg/mL) and SEITU (2.5, 5, 7.5, 10, and 12.5 µg/mL) was used as the reference. The enzyme solution 50 Unit (100 µL) was dissolved with dH_2O (3.9 mL) resulting in a 12.5 U/mL iNOS, 10 µL, assay buffer (25 µL), and test samples (5 µL) were injected in 96-plate well and pre-incubated at 22 ± 2°C for 15 min. The plate was incubated at 37°C for 60 min. A 200 µL quantity of NO detection reagent was added, the detection reaction was run at 37°C for 60 min, and absorbance was determined at a wavelength of 500–570 nm using an Elisa plate reader (ThermoFisher Scientific) at 540 nm. The average of five readings was used to calculate the percentage of iNOS inhibition using the following formula:

$$\%\,Inhibition = \left(1 - \frac{\Delta OD_{Test\ Cpd}}{\Delta OD_{NO\ inhibitor}}\right) \times 100\%$$

Where $\Delta OD_{\text{Test Cpd}}$ is the OD540 value of a test compound subtracted by the OD540 value of the blank well (without substrate) at 60 min, and $\Delta OD_{\text{NO inhibitor}}$ is the OD540 value of the control subtracted by the OD540 value of the blank well (without substrate) at 60 min. The IC_{50} values and standard deviation were determined from the nonlinear regression dose–response curve.

Results

The Nutritional Composition, Vitamin C, Total Anthocyanins, C3G, and Rutin Levels in EEIE

Determination of nutritional composition revealed that EEIE contains protein 21.81%, fat 0.99%, carbohydrate 38.27%, water 24.56%, and ash 14.37%. The total anthocyanins and vitamin C levels were 47.535 mg/100 g and 985.250 mg/100 g, respectively.

The thin-layer chromatography bands of EEIE are depicted in Figure 2. C3G was measured at 570 nm and eluted at a retention factor of Rf 0.76 ± 0.02, while quercetin was measured at 280 nm and eluted at Rf 0.55 ± 0.01, thus confirming the presence of considerable amounts of C3G and quercetin in EEIE (Figure 2a and b, respectively). The levels of the C3G and quercetin were calculated using the linear regression equation for C3G (y = 458.68 x – 1617.9; R = 0.955) resulting in 7.97 µg/mg and quercetin (y = 92.55 x – 1051.3; R = 0.992) resulting in 41.55 µg/mg.

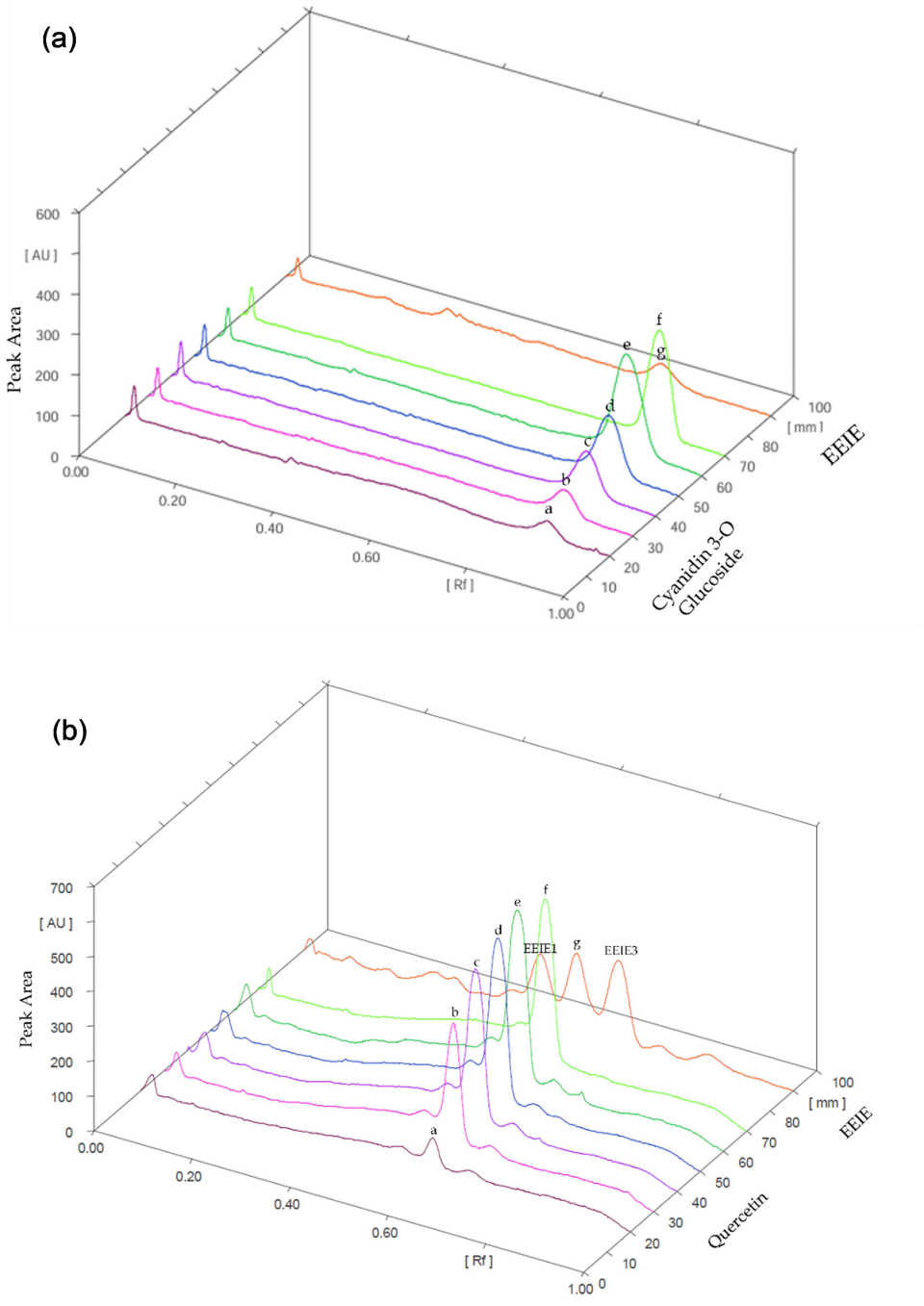

Figure 2 TLC-densitometry chromatograms of (**a**) standard C3G and C3G in EEIE; (**b**) standard quercetin and quercetin in EEIE. (**a-f** peaks indicate the spiked standards in increasing concentration, and the g peak indicates the assayed constituent in EEIE).

https://doi.org/10.2147/JEP.S505658

In silico Pharmacology in Terms of Drug-Likeness Profile, Binding Mode, Binding Affinity, and ADMET Properties

The drug-likeness profile, binding mode, and binding affinity of phytoconstituents of *E. elatior* inflorescence compared to SEITU and quinazoline, known inhibitors of human iNOS, are presented in Table 1. Moreover, the flavylium cation form of cyanidin was also studied. Of those, the best affinity is shown by, respectively, the flavylium cation of cyanidin, demethoxycurcumin, C3G, cyanidin, rutin, quercetin, luteolin, apigenin, kaempferol, and myricetin, all of which are better than the known inhibitors. The binding modes are depicted in Figure 3.

The prediction of ADMET properties of C3G, cyanidin, rutin, quercetin, and luteolin using the pkCSM program (https://biosig.lab.uq.edu.au/pkcsm/prediction_single) is tabulated in Table 2. The absorption properties of flavonoids were measured by three parameters: water solubility, human intestinal absorption (HIA), and Caco2 permeability (Table 2). The distribution property of the flavonoids was measured by two parameters, ie, the volume of distribution at steady state (VDss) and plasma protein binding (PPB) (Table 2). In this study, only cyanidin shows an almost normal VDss value of 0.952 L/kg and only four flavonoids show a good PPB value, ranging from 73.37 to 99.72%. The metabolism property of the flavonoids was predicted by their capability to influence CYP2D6 and CYP3A4 (Table 2). In this study, only quercetin may potentially inhibit CYP2D6. The elimination property of the flavonoids was predicted by measuring two parameters: clearance and OCT2 (Renal Organic Cation Transporter 2) (Table 2). The total clearance value of the flavonoids ranges from −0.369 to 0.548 indicating the possibility to be reabsorbed. Furthermore, the toxicity of the flavonoids was predicted by measuring the Ames toxicity score and the LD_{50} (Table 2). None of the flavonoids in this study exhibited mutagenic or carcinogenic potential, with LD_{50} values ranging between 2.455 and 2.547 mg/kg.

The Dynamics Stability of the Ligand-iNOS Complex

The dynamic stability of C3G/iNOS within 100 ns was determined using MD simulation and compared to that of quinazoline/iNOS. The resulting RMSD and RMSF graphs are shown in Figure 4.

The complexes C3G/iNOS (red graph in Figure 4a) exhibited a slight increase of RMSD at 5 ns indicating the flexibility of the complex in the initial conformation which interestingly is similar to that of quinazoline/iNOS (black graph in Figure 4a). However, a stable backbone conformation of both complexes is observed during 10 to 55 ns of MD simulation, with an average RMSD value of <0.25 Å (Table 3). Unexpectedly, the C3G/iNOS was unstable at 75–100 ns with an RMSD value of 0.35 Å, but the hydrogen bond with Glu377 was tightly maintained (Table 3).

Meanwhile, in Figure 4b the RMSF pattern of C3G/iNOS (red graph in Figure 4b) and quinazoline/iNOS (black graph in Figure 4b) within 100 ns simulation resulted in similar flexible regions on residues 110–140, 150–160, 175, 255, 260–275, 320–340, and 390–410.

Solvent Accessible Surface Area and Radius of Gyration

The SASA and Rg graphs are shown in Figure 5. The SASA was computed for 100 ns of MD trajectory simulation. The SASA graphs reveal similar patterns of C3G/iNOS (the purple graph in Figure 5a), demethoxycurcumin/iNOS (blue graph in Figure 5a), and quercetin/iNOS (orange graph in Figure 5a), with SEITU/iNOS (black graph in Figure 5a) and quinazoline/iNOS (yellow graph in Figure 5a) complexes, thus further confirming that these three phytoconstituents may function as potential inhibitors of human iNOS. In this study, the Rg graphs revealed similar patterns between C3G/iNOS (purple graph in Figure 5b), demethoxycurcumin/iNOS (the blue graph in Figure 5b), cyanidin/iNOS (green graph in Figure 5b) and quercetin/iNOS (the orange graph in Figure 5b), with SEITU/iNOS (black graph in Figure 5b) and quinazoline/iNOS (yellow graph in Figure 5b) complexes.

The Inhibitory Activity of EEIE on Human iNOS

The computational study was validated using an in vitro inhibitory activity of EEIE on human iNOS. EEIE inhibited human iNOS (Figure 6A) with an IC_{50} value of 24.718 µg/mL; meanwhile, for SEITU (a known inhibitor for iNOS), the IC_{50} value was 6.930 µg/mL (Figure 6B).

Table 1 The Drug-Likeness Profile, Binding Affinity, and Interaction of Eight Phytoconstituents in *E. elatior* Inflorescence With Human iNOS

Name of the Ligand or Plant Metabolite	2D Structure	Molecular Weight (g/mol)	cLogP (should be < 5)	Number of HBAs (should be < 10)	Number of HBDs (should be < 5)	Binding Energy in kcal/mol	Inhibition Constant (Ki) in μM	Hydrogen Bond (HB) with Important Residues	Interaction with Other Residues
Quercetin ($C_{15}H_{10}O_7$; PubChem CID 5280343)	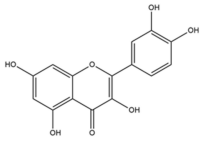	302.23	0.5243	7	5	−7.44	3.78	Glu377, Trp372	HB with Trp194, Cys200, Gly202 Hydrophobic with Trp194, Cys200, Pro350, Phe369, Asn370, Gly371
Rutin ($C_{27}H_{30}O_{16}$; PubChem CID 5280805)	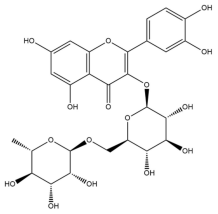	610.52	1.8385	16	10	−7.59	2.71	Glu377, Trp372	HB with Cys200, Gly202, Asn370 Hydrophobic with Trp194, Ala197, Arg199, Cys200, Phe369
Cyanidin ($C_{15}H_{11}O_6$; PubChem CID 128861)	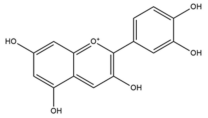	287.24	0.7661	6	5	−7.61	2.64	Glu377, Trp372	HB with Ser242, Val352, Gly371, Trp372 Hydrophobic with Trp372, Pro350
Flavylium cation ($C15H11O^+$; PubChem CID 145858)	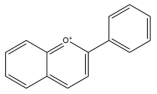	196.00	1.1509	0	1	−9.32	0.15	Trp372	No other HB interactions Hydrophobic with Trp194, Cys200, Leu209, Phe369

(*Continued*)

https://doi.org/10.2147/JEP.S505658

Table 1 (Continued).

Name of the Ligand or Plant Metabolite	2D Structure	Molecular Weight (g/mol)	cLogP (should be < 5)	Number of HBAs (should be < 10)	Number of HBDs (should be < 5)	Binding Energy in kcal/mol	Inhibition Constant (Ki) in μM	Hydrogen Bond (HB) with Important Residues	Interaction with Other Residues
C3G ($C_{21}H_{21}O_{11}$; PubChem CID 441667)	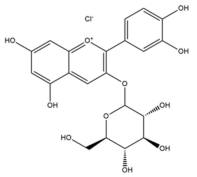	449.40	1.2628	11	8	−8.10	1.15	Glu377, Trp372	HB with Arg199, Gly202, Gly371, Asn370, Tyr489 Hydrophobic with Trp194, Ala197, Arg199, Cys200, Phe369
Kaempferol ($C_{15}H_{10}O_6$; PubChem CID 5280863)	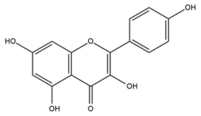	286.24	0.6461	6	4	−7.31	4.42	Glu377, Trp372	HB with Arg199, Cys200, Asn370 Hydrophobic with Trp194, Cys200, Ile201
SEITU S-ethyl isothiourea ($C_3H_8N_2S$; PubChem CID 5139)	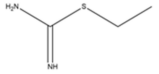	104.18	0.9222	2	0	−3.31	3.78	Glu377, Trp372	No other HB interaction Salt Bridge with Glu377 Hydrophobic with Pro350, Val352
Quinazoline ($C_8H_6N_2$; PubChem CID 9210)	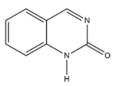	130.15	1.6298	2	0	−5.70	66.76	Trp372	HB with Gly371 Hydrophobic with Trp372, Met434, Ala439

https://doi.org/10.2147/JEP.S505658

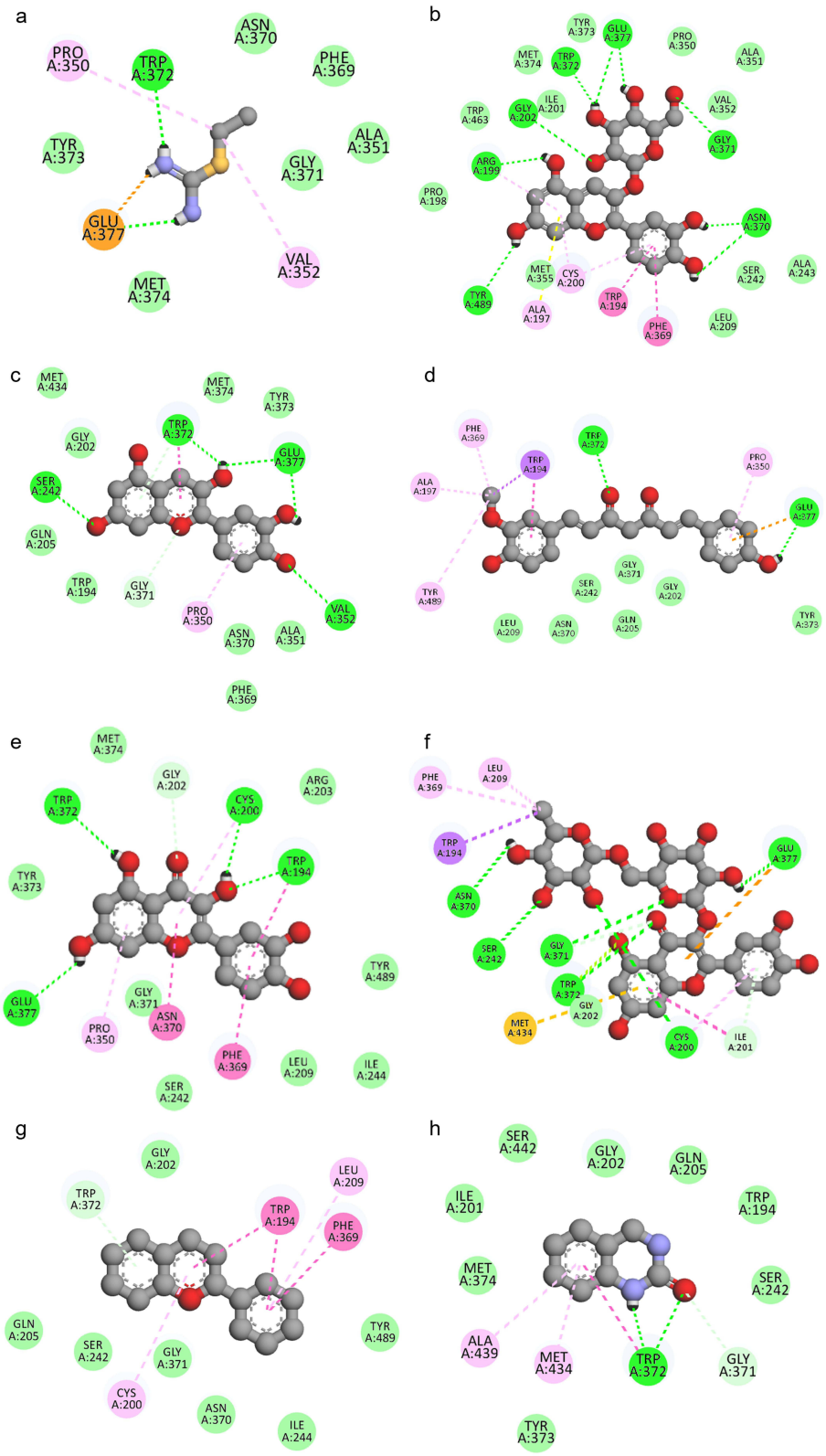

Figure 3 The binding mode of (**a**) SEITU, (**b**) C3G, (**c**) cyanidin, (**d**) demethoxycurcumin, (**e**) quercetin, (**f**) rutin, (**g**) flavylium cation, and (**h**) quinazoline. SEITU, C3G, cyanidin, demethoxycurcumin, quercetin, and rutin interact with Glu377 in the catalytic pocket of human iNOS. Hydrogen bonds are shown as green dashed lines. Left figures are the binding mode in 2D visualization. Right figures are the binding mode in 3D visualization.

https://doi.org/10.2147/JEP.S505658

Table 2 ADMET Prediction of Five Flavonoids With the Best Affinity to Human iNOS

Name of Compound	Absorption			Distribution		Metabolism		Excretion		Toxicity	
	Water Solubility (mol/L)	HIA (%)	Caco2 (Log Papp in cm/s)	VDss (L/kg)	PPB (%)	CYP3A4 Inhibitor	CYP2D6 Inhibitor	Clearance	OCT2	Ames Toxicity	LD_{50} (mg/kg)
Phytoconstituents											
C3G	−2.904	29.93	0.26	1.490	73.37	No	No	0.548	No	No	2.55
Cyanidin	−2.935	87.30	−0.35	0.952	100	No	No	0.532	No	No	2.46
Flavylium cation	−2.892	100	0.642	0.011	97.80	No	No	−0.508	No	Yes	2.48
Rutin	−2.892	23.45	−0.95	1.663	75.26	No	No	−0.369	No	No	2.49
Quercetin	−2.925	77.21	−0.23	1.559	93.24	No	Yes	0.407	No	No	2.47
iNOS inhibitor											
Quinazoline	−1.099	97.30	1.491	−0.249	97.02	No	No	0.830	No	No	2.42
SEITU	−0.363	85.51	1.211	−0.287	87.31	No	Yes	0.248	No	No	2.54

Abbreviations: HIA, Human Intestinal Absorption; Caco2, Cancer-Coli 2; VDss, Volume of Distribution at Steady State; PPB, Protein Plasma Binding; CYP2D6, Cytochrome P450 subfamily 2D6; CYP3A4, Cytochrome P450 subfamily 3A4; OCT2, Renal Organic Cation Transporter 2; LD_{50}, Lethal $Dose_{50}$; the dose that causes lethality in 50% of the test subjects.

Discussion

In the present study, the determination of nutritional composition revealed that the ethanol extract of *E. elatior* inflorescence petals collected from West Java, Indonesia, contains protein 21.81%, fat 0.99%, carbohydrate 38.27%, water 24.56%, and ash 14.37%. In comparison with our study, the nutritional composition of *E. elatior* inflorescence collected from Penang, Malaysia, showed a significant amount of crude protein 12.6%, fat 18.2%, fiber 17.6%, and essential amino acids dominated by leucine 7.2% and lysine 7.9%. The inflorescence also contained minerals such as

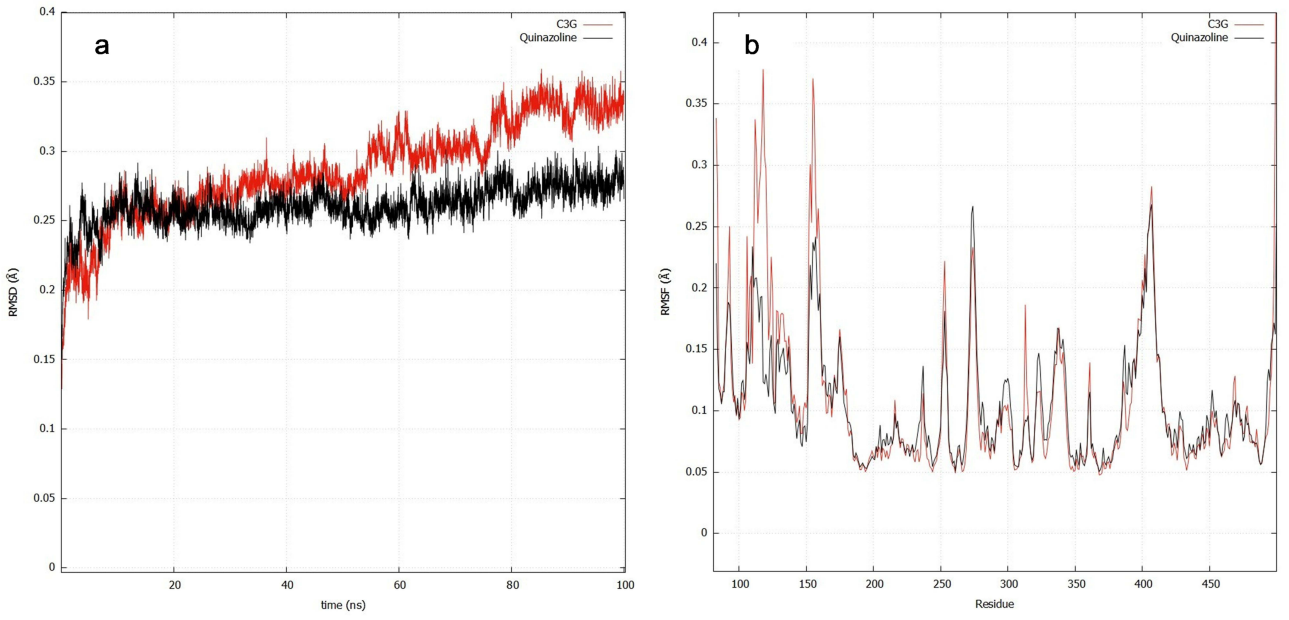

Figure 4 The RMSD (**a**) and RMSF (**b**) graphs of C3G (red) and quinazoline (black) in complex with iNOS within 100 ns MD simulation. In the left (**a**) graph, the x-axis indicates the RMSD value in Å and the y-axis indicates time in ns. In the right (**b**) graph, the x-axis indicates the RMSF value in Å and the y-axis indicates the amino acid residue.

Table 3 Hydrogen Bond Interaction Between C3G With Human iNOS During 100 ns MD Simulation

Time	3D Visualization	2D Visualization	Hydrogen Bond
0 ns	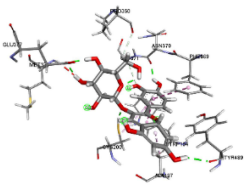	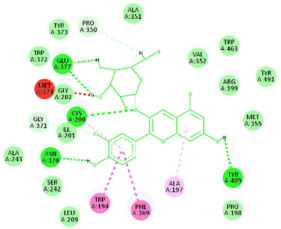	Glu377; Cys200; Asn370; Tyr489
20 ns	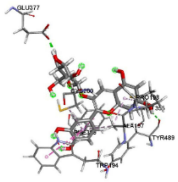	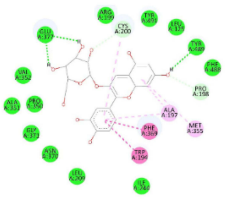	Glu377; Tyr489
40 ns	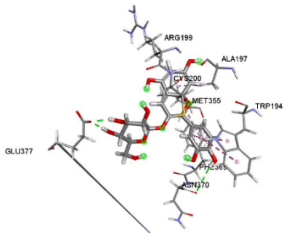	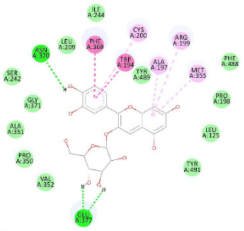	Glu377; Asn370
60 ns	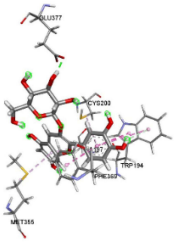	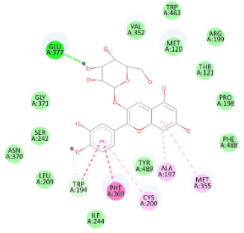	Glu377
80 ns	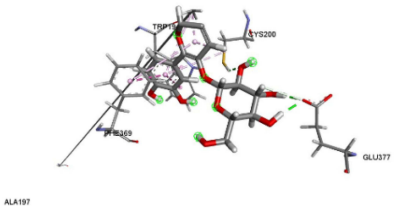	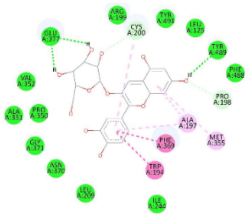	Glu377; Tyr489
100 ns	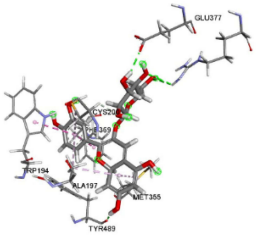	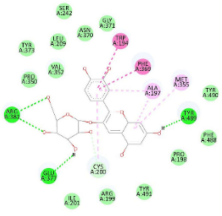	Glu377; Arg381; Tyr489

https://doi.org/10.2147/JEP.S505658

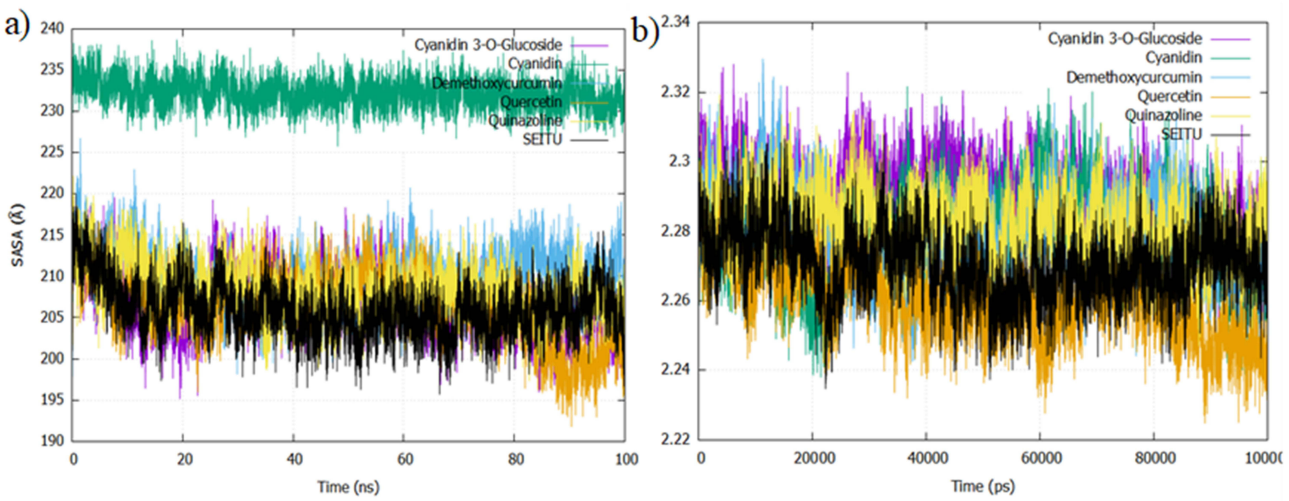

Figure 5 The (**a**) solvent accessible surface area (SASA) and (**b**) radius of gyration (Rg) plot of EEIE phytoconstituent and iNOS inhibitors within 100 ns MD simulation. In the left (**a**) graph, the x-axis indicates the solvent accessible area in nm^2 and the y-axis indicates time in ns. In the right (**b**) graph, the x-axis indicates the radius of the gyration in Å and the y-axis indicates the time in ps.

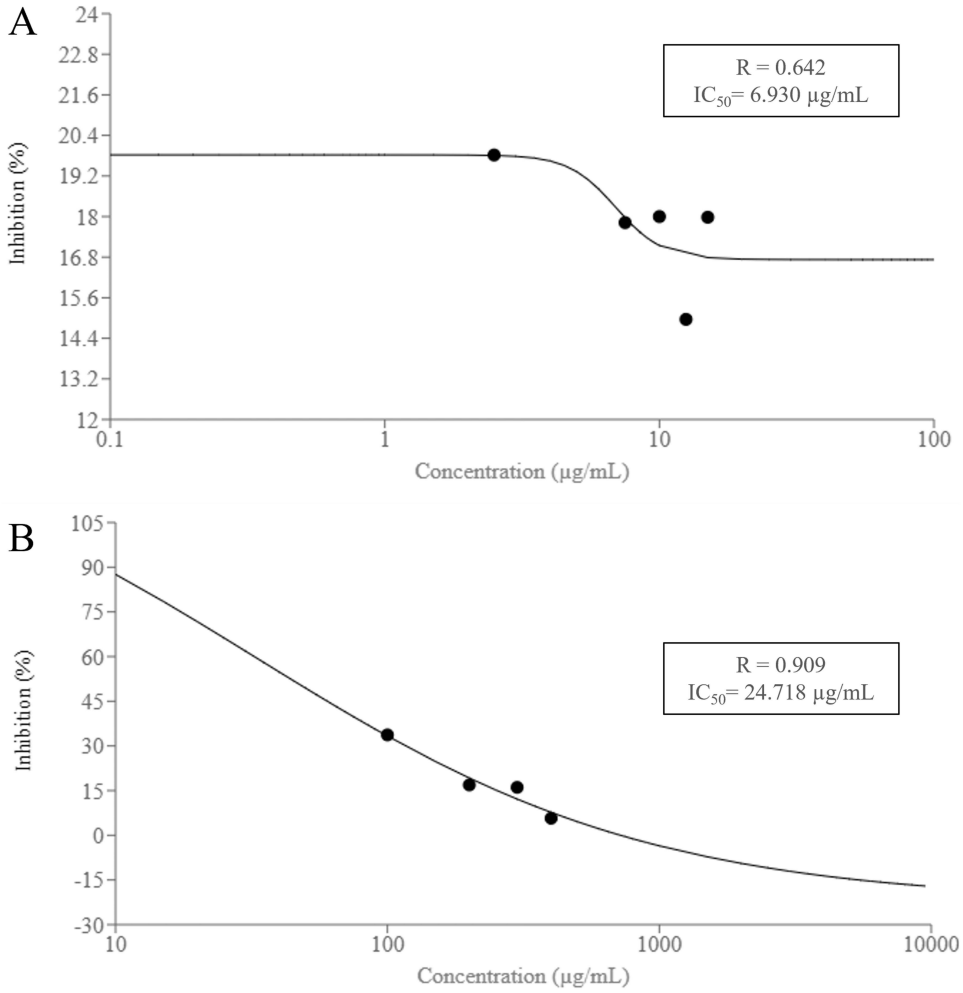

Figure 6 Inhibitory activity of (**A**) SEITU (IC_{50}= 6.930 µg/mL) and (**B**) EEIE (IC_{50}= 24.718 µg/mL) towards human iNOS (Catalogue No. EINO-100; EnzyChrom-BioAssay) by in vitro study.

potassium, calcium, magnesium, phosphorous, and sulfur.[54] Another study of the flowers of *E. elatior* collected from Thailand reported the percentage of protein 0.44 ± 0.00%, fat 0.37 ± 0.02%, carbohydrate 2.46 ± 0.12%, fiber 0.96 ± 0.06%, ash 0.65 ± 0.05%, and water 95.12 ± 0.35%.[55]

In our present study, the total anthocyanins and vitamin C levels were 47.535 mg/100 g and 985.250 mg/100 g, respectively. The vitamin C levels were determined based on the sour taste of the extract. The levels of vitamin C in *E. elatior* plants were scarcely reported; however, a study delineated that the flowers of *E. elatior* collected from Thailand contained a low amount of vitamin C of 1.05 ± 0.03 mg/100 g extract and total flavonoids of 42.50 ± 2.64 mg rutin equivalence/g extract.[55] Vitamin C at a concentration of 0.36% was also reported by Anzian et al to be present in the flowers of *E. elatior* collected from Selangor, Malaysia.[56]

Furthermore, the TLC-densitometry chromatograms confirms the presence of C3G and quercetin in EEIE in considerable amounts (C3G is 7.97 µg/mg, and quercetin 41.55 µg/mg). A previous study reported that kaempferol, quercetin, rutin, quercitrin, isoquercitrin, and other compounds were detected in *E. elatior* flowers collected in the Songkhla Province, Southern Thailand.[56] The methanol extract of E. elatior flowers collected in Penang, Malaysia, showed total anthocyanins of 5.9 mg C3GE per 100 g extract.[23] Considering that EEIE contains quercetin and anthocyanins, we performed a computational study of these phytoconstituents towards human iNOS.

The water solubility of a drug reflects its solubility in water at 25°C. Our study revealed that the phytoconstituents of *E. elatior* inflorescence possess good water solubility, and thus may be easily absorbed and excreted by the urinary system. The HIA values of cyanidin and luteolin were comparable to those of SEITU and quinazoline, which is >80%, indicating their good absorbability in the gastrointestinal system. HIA is categorized as one of the most important ADME properties, showing one of the key steps during the transport of drugs to their site of action.[57] Furthermore, all flavonoids of *E. elatior* inflorescence and iNOS inhibitors exhibit good Caco2 permeability with Log Papp values ranging from −0.95 to 1.491 cm/s. Caco2 cells are human colon epithelial cancer cell lines that are used as a model of human intestinal absorption of drugs because they resemble the human intestinal epithelium. The apparent permeability coefficient (Papp) was calculated from the permeation rate and compound concentration at time 0 h and time 2 h. Drugs with high (70–100%) in vivo absorption should have a Log Papp value > 8×108 cm/s or > 0.9 cm/s.[58]

The volume of distribution (VD) is a pharmacokinetic parameter that represents the tendency of a drug to either remain in the plasma or redistribute to other tissue compartments. Drugs with a high VD tend to leave the plasma and enter extravascular compartments of the body, thus requiring a higher dose to achieve a given plasma concentration. At a steady state (VDss), the net flux of the drug between the central and peripheral compartments is 0.[59,60] It is considered normal when the VDss value ranges from 0.04 to 0.7 L/kg.[61,62]

The plasma protein binding (PPB) prediction is important in the pharmacokinetics characterization of drugs because it causes significant changes in the VD, clearance, and half-life of a drug.[63] PPB is the reversible association of a drug with the plasma proteins due to hydrophobic and electrostatic interactions, such as Van der Waals and hydrogen bonds. The fraction of bound drugs exists in equilibrium with the fraction of unbound drugs. Only a fraction of unbound drugs can pass across cell membranes.[64] The higher the PPB percentage of a drug, the lower the fraction of unbound drug available for therapeutic effect.[65]

All xenobiotics undergo a biotransformation process. Hepatic enzymes, the subfamilies of cytochrome P450, metabolize and convert drugs to more polar metabolites which are eventually eliminated. CYP2D6 and CYP3A4 contribute to 2% of the overall hepatic CYP450 enzyme and are responsible for the metabolism of 25% of commonly prescribed drugs.[65] Drug clearance is a combination of hepatic and renal clearance related to bioavailability. OCT2 is a renal uptake transporter that functions in the disposition and clearance of drugs.[66] It is defined that the clearance value of <0.67 is reabsorbed, between 0.67 and 1.5 is intermediate (not reabsorbed and may be secreted), and >1.5 is secreted.[67] The toxicity of the flavonoids is predicted by measuring the Ames toxicity score and LD50. AMES Toxicity is commonly used to evaluate the mutagenic potential of a drug, indicating that when the results are positive, the studied drug is mutagenic and could behave as a carcinogen.[68]

The substrate of NOS, L-arginine, attaches to the narrow part of the catalytic site cavity with the guanidino group lying coplanar to the heme and builds two hydrogen bonds to both carboxy oxygens of Glu377, thus making this residue critical for substrate binding.[11] Our in silico pharmacology study confirms that C3G, an anthocyanin of *Etlingera elatior* inflorescence, occupies the catalytic site of human iNOS and binds to Glu377 (binding energy of −8.10 kcal/mol).

Moreover, during the 100 ns molecular dynamic simulation, the hydrogen bond between C3G and Glu377 was not disrupted (Table 1 and Table 3), confirming the stability of the complex. Despite the instability of the C3G/iNOS complex beginning at 75 to 100 ns with an RMSD value of a maximum of 0.35 Å (Figure 4a), the hydrogen bond with Glu377 is tightly kept (Table 3). A ligand-protein complex is defined as stable when the protein shows minimal deviation from its backbone during simulation.[68]

The RMSF pattern of C3G/iNOS and quinazoline/iNOS within the 100 ns simulation resulted in similar flexible regions on residues 110–140, 150–160, 175, 255, 260–275, 320–340, and 390–410 (Figure 4b), which is similar to a previous MD simulation by Zhang et al which confirmed four major flexible protein segments in iNOS corresponding to residues 264–272, 327–337, 370–380, and 389–409. Key amino acids in the catalytic pocket of iNOS are Met368, Trp366, Gly365, Tyr367, Phe363, Pro344, Gln257, Val346, Asn364, Met349, Thr370, Glu371, and Tyr485, and the activities of iNOS inhibitors are consistent with their ability to alter the position of these important residues.[69] RMSF in MD simulation is used to identify the flexible regions of the protein-ligand complexes and less-stable proteins will show higher RMSF fluctuations.[68]

In this study, we calculated protein solvent accessible surface area (SASA). SASA is the region around a protein by the Van der Waals contact surface of the molecule and a hypothetical center of a solvent sphere.[70] The last parameter in the MD simulation is the radius of gyration (Rg), which is employed to predict the compactness manner, and flexibility of the protein inside a biological environment. Lower values of Rg indicate a more rigid structure during the simulation.[71] Our study confirms that the SASA and Rg graphs (Figure 5) of the phytoconstituents C3G/iNOS, cyanidin/iNOS, demethoxycurcumin/iNOS, and quercetin/iNOS complexes were similar to those of the iNOS inhibitors (quinazoline/iNOS and SEITU/iNOS) complexes.

The present study confirmed that EEIE inhibited human iNOS with an IC_{50} value of 24.718 µg/mL, which is weaker than that of SEITU (a known inhibitor for iNOS), with an IC_{50} value of 6.930 µg/mL. The in vitro results are in line with the computational study. Inhibition of iNOS may be attributed to the presence of flavonoids and anthocyanins in EEIE.

Anthocyanins are broadly distributed in plants, especially in dark-colored flowers, berries, and vegetables. These plant metabolites, belonging to the flavonoid family, have been explored for their ability to alleviate inflammation via numerous pathways.[72–76] Pelargonidin-3-o-glucoside, an anthocyanin found in strawberries, significantly prevented the translocation of NF-kappaB p65 to the nucleus.[72] Anthocyanins inhibited both the activity and production of various pro-inflammatory important substances and enzymes, such as TNF-α, NO, iNOS, COX-2, and lipoxygenase (LOX).[73] C3G contained in *Oryza sativa* L. could inhibit the translocation of NF-kappaB p50 and p65 in mucositis rat models and oral keratinocyte cultures.[74] Anthocyanins show anti-inflammatory effects in animal models with ulcerative colitis.[75] Other anthocyanin, delphinidin 3-sambubioside, reduced iNOS/NO, IL-6, and TNF-α.[76]

Conclusion

Plants such as *Etlingera elatior* flowers (inflorescences) may have the potential as sources of essential nutrients, such as protein 21.81%, fat 0.99%, carbohydrate 38.27%, water 24.56%, and ash 14.37%. The total anthocyanin and vitamin C levels in the ethanol extract of *E. elatior* inflorescence were 47.535 mg/100 g and 985.250 mg/100 g, respectively. Anthocyanins are of interest because of their numerous pharmacology activities. In this study, C3G, cyanidin, and the flavylium cation of cyanidin showed strong binding affinity to human iNOS. Interestingly, all flavonoids can occupy the catalytic site by binding to Glu377 and Trp372, similar to SEITU and quinazoline, which are inhibitors of human iNOS. The affinity of C3G was comparable to that of quinazoline, as evidenced by the binding modes, and RMSD, RMSF, SASA, and Rg calculations. The computational results aligned with the in vitro study and confirmed that the ethanol extract of *E. elatior* inflorescence inhibited human iNOS with an IC50 value of 24.718 µg/mL, although the inhibition is weaker than that of SEITU (a known inhibitor for iNOS). Therefore, *E. elatior* inflorescence may be developed as an anti-inflammatory agent whose activity is attributed to the anthocyanins.

Data Sharing Statement

The data generated in the present study may be requested from the first author upon reasonable request.

Acknowledgments

The authors thank the Republic of Indonesia Ministry of Education and Culture and the Rector of Universitas Padjadjaran via the Directorate of Research and Community Engagement.

Funding

The tuition fee and living cost of the first author are funded by the Republic of Indonesia Ministry of Education and Culture via the PMDSU (Program Magister Doktor Sarjana Unggul) Scholarship years 2023 and 2024. The purchase of cyanidin 3-glucoside chloride (Item No. 16406; Cayman Chemical), plant materials, extraction solvent, proximate analysis, total anthocyanin levels, and TLC-densitometry, were funded by the Rector of Universitas Padjadjaran via the Directorate of Research and Community Engagement in the scheme of Academic-Leadership Research Grant No. 1479/UN6.3.1/PT.00/2024 of Prof. Dr. Jutti Levita. The APC was funded by the Rector of Universitas Padjadjaran via the Directorate of Research and Community Engagement.

Disclosure

The authors declare that they have no known competing financial interests or personal relationships that could influence the work reported in this article.

References

1. Chan FK, Leung WK. Peptic-ulcer disease. *Lancet*. 2002;360(9337):933–941. doi:10.1016/s0140-6736(02)11030-0
2. Lanas A, Chan FKL. Peptic ulcer disease. *Lancet*. 2017;390(10094):613–624. doi:10.1016/s0140-6736(16)32404-7
3. Malik TF, Gnanapandithan K, Singh K. Peptic Ulcer Disease. 2023. In: *StatPearls*. Treasure Island (FL): StatPearls Publishing; PMID: 30521213.
4. Groenen MJ, Kuipers EJ, Hansen BE, Ouwendijk RJ. Incidence of duodenal ulcers and gastric ulcers in a Western population: back to where it started. *Can J Gastroenterol*. 2009;23(9):604–608. doi:10.1155/2009/181059
5. Sung JJ, Kuipers EJ, El-Serag HB. Systematic review: the global incidence and prevalence of peptic ulcer disease. *Aliment Pharmacol Ther*. 2009;29(9):938–946. doi:10.1111/j.1365-2036.2009.03960.x
6. Li Z, Zou D, Ma X, et al. Epidemiology of peptic ulcer disease: endoscopic results of the systematic investigation of gastrointestinal disease in China. *Am J Gastroenterol*. 2010;105(12):2570–2577. doi:10.1038/ajg.2010.324
7. Bhattacharyya A, Chattopadhyay R, Mitra S, Crowe SE. Oxidative stress: an essential factor in the pathogenesis of gastrointestinal mucosal diseases. *Physiol Rev*. 2014;94(2):329–354. doi:10.1152/physrev.00040.2012
8. Peek RM Jr, Fiske C, Wilson KT. Role of innate immunity in *Helicobacter pylori*-induced gastric malignancy. *Physiol Rev*. 2010;90(3):831–858. doi:10.1152/physrev.00039.2009
9. Bredt DS, Snyder SH. Isolation of nitric oxide synthetase, a calmodulin-requiring enzyme. *Proc Natl Acad Sci USA*. 1990;87(2):682–685. doi:10.1073/pnas.87.2.682
10. Barrachina MD, Panés J, Esplugues JV. Role of nitric oxide in gastrointestinal inflammatory and ulcerative diseases: perspective for drugs development. *Curr Pharm Des*. 2001;7(1):31–48. doi:10.2174/1381612013398491
11. Alderton WK, Cooper CE, Knowles RG. Nitric oxide synthases: structure, function, and inhibition. *Biochem J*. 2001;357:593–615. doi:10.1042/bj3570593
12. Fischmann TO, Hruza A, Niu XD, et al. Structural characterization of nitric oxide synthase isoforms reveals striking active-site conservation. *Nat Struct Biol*. 1999;6:233–242. doi:10.1038/6675
13. Matsuda H, Morikawa T, Ando S, Toguchida I, Yoshikawa M. Structural requirements of flavonoids for nitric oxide production inhibitory activity and mechanism of action. *Bioorg Med Chem*. 2003;11(9):1995–2000. doi:10.1016/s0968-0896(03)00067-1
14. Khallaf ISA, Bayoumi SAL, Malak LG, et al. The inhibition of inducible nitric oxide production in lipopolysaccharide-stimulated rat macrophages and in silico studies by flavonoids from Iris spuria L. rhizomes. *J Ethnopharmacol*. 2021;278:114311. doi:10.1016/j.jep.2021.114311
15. Qian Y, Babu P, Symons J, et al. Metabolites of flavonoid compounds preserve indices of endothelial cell nitric oxide bioavailability under glucotoxic conditions. *Nutr Diabetes*. 2017;7:e286. doi:10.1038/nutd.2017.34
16. Chen YC, Shen SC, Lee WR, Hou WC, Yang LL, Lee TJ. Inhibition of nitric oxide synthase inhibitors and lipopolysaccharide-induced inducible NOS and cyclooxygenase-2 gene expressions by rutin, quercetin, and quercetin pentaacetate in RAW 264.7 macrophages. *J Cell Biochem*. 2001;82(4):537–548. doi:10.1002/jcb.1184
17. Levita J, Patala R, Kolina J, et al. Pharmacophore modeling and molecular docking of phytoconstituents in Morus sp. and *Arcangelisia flava* against nitric oxide synthase for antiinflammatory discovery. *J Appl Pharm Sci*. 2018;8(12):053–059. doi:10.7324/JAPS.2018.81207
18. Alshehri B, Vijayakumar R, Senthilkumar S, et al. Therapeutic potential of nitric oxide synthase inhibitor from natural sources for the treatment of ischemic stroke. *Saudi J Biol Sci*. 2022;29(2):984–991. doi:10.1016/j.sjbs.2021.10.003
19. Singh SP, Konwar BK. Molecular docking studies of quercetin and its analogues against human inducible nitric oxide synthase. *Springerplus*. 2012;1(1):69. doi:10.1186/2193-1801-1-69
20. Maimulyanti A, Prihadi AR. Chemical composition, phytochemical and antioxidant activity from extract of *Etlingera elatior* flower from Indonesia. *J Pharmacogn Phytochem*. 2015;3(6):233–238.
21. Chan EWC, Lim YY, Wong SK. Phytochemistry and pharmacological properties of *Etlingera elatior*: a review. *Pharmacogn J*. 2011;3(22):6–10. doi:10.5530/pj.2011.22.2

22. Miean KH, Mohamed S. Flavonoid (myricetin, quercetin, kaempferol, luteolin, and apigenin) content of edible tropical plants. *J Agric Food Chem*. 2001;49(6):3106–3112. doi:10.1021/jf000892m
23. Wijekoon MMJO, Bhat R, Karim AA. Effect of extraction solvents on the phenolic compounds and antioxidant activities of bunga kantan (*Etlingera elatior* Jack.) inflorescence. *J Food Comp Anal*. 2011;24(4–5):615–619. doi:10.1016/j.jfca.2010.09.018
24. Juwita T, Pakpahan W HP, Puspitasari I M, Mekar Saptarini N, Levita J. Anti-inflammatory activity of Etlingera elatior (Jack) R.M. Smith flower on gastric ulceration-induced Wistar rats. *Pak J Biol Sci*. 2020;23(9):1193–1200. doi:10.3923/pjbs.2020.1193.1200
25. Backer CA, Bakhuizen van den Brink RC. *Flora of Java (Spermatophytes Only)*. Vol. III. Groningen: N.V.P. Noordhoff; 1968.
26. Poulsen AD. *Etlingera* Giseke of Java. *Gard Bull Singapore*. 2007;59(1–2):145–172.
27. Jackie T, Haleagrahara N, Chakravarthi S. Antioxidant effects of Etlingera elatior flower extract against lead acetate - induced perturbations in free radical scavenging enzymes and lipid peroxidation in rats. *BMC Res Notes*. 2011;4:67. doi:10.1186/1756-0500-4-67
28. Official Methods of Analysis 22nd edition. 2023. Available from: https://www.aoac.org/official-methods-of-analysis/. Accessed January 2024.
29. Abeysuriya HI, Bulugahapitiya VP, Loku Pulukkuttige J. Total vitamin C, ascorbic acid, dehydroascorbic acid, antioxidant properties, and iron content of underutilized and commonly consumed fruits in Sri Lanka. *Int J Food Sci*. 2020;2020:4783029. doi:10.1155/2020/4783029
30. Taghavi T, Patel H, Rafie R. Comparing pH differential and methanol-based methods for anthocyanin assessments of strawberries. *Food Sci Nutr*. 2021;10(7):2123–2131. doi:10.1002/fsn3.2065
31. Doshi GM, Une HD. Quantification of quercetin and rutin from *Benincasa hispida* seeds and Carissa congesta roots by high-performance thin layer chromatography and high-performance liquid chromatography. *Pharmacogn Res*. 2016;8(1):37–42. doi:10.4103/0974-8490.171098
32. Skaar I, Adaku C, Jordheim M, Byamukama R, Kiremire B, Øm A. Purple anthocyanin colouration on lower (abaxial) leaf surface of Hemigraphis colorata (Acanthaceae). *Phytochemistry*. 2014;105:141–146. doi:10.1016/j.phytochem.2014.05.016
33. Aulifa DL, Adnyana IK, Sukrasno S, Levita J. Inhibitory activity of xanthoangelol isolated from Ashitaba (*Angelica keiskei* Koidzumi) towards α-glucosidase and dipeptidyl peptidase-IV: *in silico* and *in vitro* studies. *Heliyon*. 2022;8(5):e09501. doi:10.1016/j.heliyon.2022.e09501
34. Wang J. Estimation of the quality of refined protein crystal structures. *Protein Sci*. 2015;24(5):661–669. doi:10.1002/pro.2639
35. Ghasemzadeh A, Jaafar HZ, Rahmat A, Ashkani S. Secondary metabolites constituents and antioxidant, anticancer and antibacterial activities of *Etlingera elatior* (Jack) R.M.Sm grown in different locations of Malaysia. *BMC Complement Altern Med*. 2015;15:335. doi:10.1186/s12906-015-0838-6
36. Juwita T, Melyani Puspitasari I, Levita J. Torch Ginger (*Etlingera elatior*): a Review on its botanical aspects, phytoconstituents and pharmacological activities. *Pak J Biol Sci*. 2018;21(4):151–165. doi:10.3923/pjbs.2018.151.165
37. Noordin L, Wan Ahmad WAN, Muhamad Nor NA, Abu Bakar NH, Ugusman A. *Etlingera elatior* flower aqueous extract protects against oxidative stress-induced nephropathy in a rat model of type 2 diabetes. *Evid Based Complement Alternat Med*. 2022;2022:2814196. doi:10.1155/2022/2814196
38. Fujiwara N, Okado A, Seo HG, Fujii J, Kondo K, Taniguchi N. Quinazoline derivatives suppress nitric oxide production by macrophages through inhibition of NOS II gene expression. *FEBS Lett*. 1996;395(2–3):299–303. doi:10.1016/0014-5793(96)01058-7
39. Camacho ME, Chayah M, García ME, et al. Quinazolinones, quinazolinthiones, and quinazolinimines as nitric oxide synthase inhibitors: synthetic study and biological evaluation. *Arch Pharm*. 2016;349(8):638–650. doi:10.1002/ardp.201600020
40. Mittal A, Arora R, Kakkar R. Pharmacophore modeling, 3D-QSAR and molecular docking studies of quinazolines and aminopyridines as selective inhibitors of inducible nitric oxide synthase. *J Theory Comput Chem*. 2019;18(1):1950002. doi:10.1142/S0219633619500020
41. Lipinski CA. Lead- and drug-like compounds: the rule-of-five revolution. *Drug Discov Today Technol*. 2004;1(4):337–341. doi:10.1016/j.ddtec.2004.11.007
42. Nath M, Bhowmik D, Saha S, Nandi R, Kumar D. Identification of potential inhibitor against *Leishmania donovani* mitochondrial DNA primase through in-silico and in vitro drug repurposing approaches. *Sci Rep*. 2024;14(1):3246.
43. Pires DE, Blundell TL, Ascher DB. pkCSM: predicting small-molecule pharmacokinetic and toxicity properties using graph-based signatures. *J Med Chem*. 2015;58(9):4066–4072. doi:10.1021/acs.jmedchem.5b00104
44. Patlewicz G, Jeliazkova N, Safford RJ, Worth AP, Aleksiev B. An evaluation of the implementation of the Cramer classification scheme in the Toxtree software. *SAR QSAR Environ Res*. 2008;19(5–6):495–524. doi:10.1080/10629360802083871
45. Mutakin SNM, Amalia R, Sumiwi SA, Megantara S, Saputri FA, Levita J. Molecular docking simulation of phenolics towards tyrosinase, phenolic content, and radical scavenging activity of some Zingiberaceae plant extracts. *Cosmetics*. 2023;10(6):149. doi:10.3390/cosmetics10060149
46. Abraham MJ, Murtola T, Schulz R, et al. GROMACS: high-performance molecular simulations through multi-level parallelism from laptops to supercomputers. *SoftwareX*. 2015;1:9–25. doi:10.1016/j.softx.2015.06.001
47. da Silva AW S, Vranken WF. ACPYPE - AnteChamber PYthon Parser interfacE. *BMC Res Notes*. 2012;5:367. doi:10.1186/1756-0500-5-367
48. George A, Mondal S, Purnaprajna M, Athri P. Review of electrostatic force calculation methods and their acceleration in molecular dynamics packages using graphics processors. *ACS Omega*. 2022;7(37):32877–32896. doi:10.1021/acsomega.2c03189
49. Wall ME, Calabró G, Bayly CI, Mobley DL, Warren GL. Biomolecular solvation structure revealed by molecular dynamics simulations. *J Am Chem Soc*. 2019;141(11):4711–4720. doi:10.1021/jacs.8b13613
50. Islam R, Parves MR, Paul AS, et al. A molecular modeling approach to identify effective antiviral phytochemicals against the main protease of SARS-CoV-2. *J Biomol Struct Dyn*. 2021;39(9):3213–3224. doi:10.1080/07391102.2020.1761883
51. Lolok N, Sumiwi SA, Muhtadi A, et al. Molecular docking and molecular dynamics studies of bioactive compounds contained in noni fruit (*Morinda citrifolia* L.) against human pancreatic α-amylase. *J Biomol Struct Dyn*. 2022;40(15):7091–7098. doi:10.1080/07391102.2021.1894981
52. Genheden S, Ryde U. The MM/PBSA and MM/GBSA methods to estimate ligand-binding affinities. *Expert Opin Drug Discov*. 2015;10(5):449–461. doi:10.1517/17460441.2015.1032936
53. Hou T, Wang J, Li Y, Wang W. Assessing the performance of the MM/PBSA and MM/GBSA methods. 1. The accuracy of binding free energy calculations based on molecular dynamics simulations. *J Chem Inf Model*. 2011;51(1):69–82. doi:10.1021/ci100275a
54. Jeevani Osadee Wijekoon MM, Bhat R, Karim AA. Evaluation of nutritional quality of torch ginger (*Etlingera elatior* Jack.) inflorescence. *Int Food Res J*. 2011;18(4):1415–1420.
55. Rachkeeree A, Kantadoung K, Suksathan R, et al. Nutritional compositions and phytochemical properties of the edible flowers from selected Zingiberaceae found in Thailand. *Front Nutr*. 2018;5:3. doi:10.3389/fnut.2018.00003

56. Anzian A, Rashidah S, Saari N, Wan sapawi CWNS C, Meor Hussin AS. Chemical composition and antioxidant activity of Torch Ginger (Etlingera elatior) flower extract. *Food Appl Biosci J*. 2017;5(1):32–49.
57. Yan A, Wang Z, Cai Z. Prediction of human intestinal absorption by GA feature selection and support vector machine regression. *Int J mol Sci*. 2008;9(10):1961–1976. doi:10.3390/ijms9101961
58. van Breemen RB, Li Y. Caco-2 cell permeability assays to measure drug absorption. *Expert Opin Drug Metab Toxicol*. 2005;1(2):175–185. doi:10.1517/17425255.1.2.175
59. Smith DA, Beaumont K, Maurer TS, Di L. Volume of distribution in drug design. *J Med Chem*. 2015;58(15):5691–5698. doi:10.1021/acs.jmedchem.5b00201
60. Mansoor A, Mahabadi N. Volume of distribution. (2023). StatPearls [Internet]: Available rom: https://www.ncbi.nlm.nih.gov/books/NBK545280/. Accessed March 04, 2025.
61. Berellini G, Lombardo F. An accurate in vitro prediction of human VDss based on the Øie–Tozer equation and primary physicochemical descriptors.3. analysis and assessment of predictivity on a large dataset. *Drug Metabol Dispos*. 2019;47(12):1380–1387. doi:10.1124/dmd.119.088914
62. Lombardo F, Obach RS, Shalaeva MY, Gao F. Prediction of volume of distribution values in humans for neutral and basic drugs using physicochemical measurements and plasma protein binding data. *J Med Chem*. 2002;45(13):2867–2876. doi:10.1021/jm0200409
63. Ghafourian T, Amin Z. QSAR models for the prediction of plasma protein binding. *Bioimpacts*. 2013;3(1):21–27. doi:10.5681/bi.2013.011
64. Jambhekar SS. Physicochemical and biopharmaceutical properties of drug substances and pharmacokinetics. In: Foye WO, editors. *Foye's Principles of Medicinal Chemistry*. New York: Lippincott Williams and Wilkins; 2008:247–250.
65. Cicali EJ, Smith DM, Duong BQ, Kovar LG, Cavallari LH, Johnson JA. A Scoping review of the evidence behind cytochrome P450 2D6 isoenzyme inhibitor classifications. *Clin Pharmacol Ther*. 2020;108(1):116–125. doi:10.1002/cpt.1768
66. Flores-Holguín N, Frau J, Glossman-Mitnik D. In silico pharmacokinetics, ADMET study and conceptual DFT analysis of two plant cyclopeptides isolated from Rosaceae as a computational peptidology approach. *Front Chem*. 2021;9:708364. doi:10.3389/fchem.2021.708364
67. Ito S, Ando H, Ose A, et al. Relationship between the urinary excretion mechanisms of drugs and their physicochemical properties. *J Pharm Sci*. 2013;102(9):3294–3301. doi:10.1002/jps.23599
68. Oubahmane M, Hdoufane I, Delaite C, Sayede A, Cherqaoui D, El Allali A. Design of potent inhibitors targeting the main protease of SARS-CoV-2 using QSAR modeling, molecular docking, and molecular dynamics simulations. *Pharmaceuticals*. 2023;16(4):608.
69. Zhang H, Zan J, Yu G, Jiang M, Liu P. A combination of 3D-QSAR, molecular docking and molecular dynamics simulation studies of benzimidazole-quinolinone derivatives as iNOS inhibitors. *Int J mol Sci*. 2012;13(9):11210–11227. doi:10.3390/ijms130911210
70. Ali S, Hassan M, Islam A, Ahmad F. A review of methods available to estimate solvent-accessible surface areas of soluble proteins in the folded and unfolded states. *Curr Protein Pept Sci*. 2014;15(5):456–476. doi:10.2174/1389203715666140327114232
71. Ghahremanian S, Rashidi MM, Raeisi K, Toghraie D. Molecular dynamics simulation approach for discovering potential inhibitors against SARS-CoV-2: a structural review. *J mol Liq*. 2022;354:118901. doi:10.1016/j.molliq.2022.118901
72. Duarte LJ, Chaves VC, Mvpds N, et al. Molecular mechanism of action of Pelargonidin-3-O-glucoside, the main anthocyanin responsible for the anti-inflammatory effect of strawberry fruits. *Food Chem*. 2018;247:56–65. doi:10.1016/j.foodchem.2017.12.015
73. Serra D, Henriques JF, Serra T, et al. An anthocyanin-rich extract obtained from Portuguese blueberries maintains its efficacy in reducing microglia-driven neuroinflammation after simulated digestion. *Nutrients*. 2020;12(12):3670. doi:10.3390/nu12123670
74. Tancharoen S, Shakya P, Narkpinit S, Dararat P, Kikuchi K. Anthocyanins extracted from Oryza sativa L. prevent fluorouracil-induced nuclear factor-κB activation in oral mucositis: in vitro and in vivo studies. *Int J mol Sci*. 2018;19(10):2981. doi:10.3390/ijms19102981
75. Li S, Wu B, Fu W, Reddivari L. The anti-inflammatory effects of dietary anthocyanins against ulcerative colitis. *Int J mol Sci*. 2019;20(10):2588. doi:10.3390/ijms20102588
76. Prabawati N B, Oktavirina V, Palma M, Setyaningsih W. Edible flowers: antioxidant compounds and their functional properties. *Horticulturae*. 2021;7(4):66. doi:10.3390/horticulturae7040066